

12 Resonant Inelastic X-ray Scattering on Elementary Excitations

Jeroen van den Brink

Institute for Theoretical Solid State Physics

IFW Dresden

Contents

1	Introduction	2
1.1	Features of RIXS as an experimental method	3
1.2	Progress of RIXS in the last decades	5
1.3	Probing elementary excitations with RIXS	6
2	The RIXS process	8
2.1	Direct and indirect RIXS	10
3	Interaction of light and matter	12
3.1	Kramers-Heisenberg cross-section	13
3.2	Scattering amplitude in dipole approximation	16
3.3	Scattering amplitude for a multipole expansion	19
4	Definition of direct/indirect RIXS	21
4.1	Effective theory for indirect RIXS	22
4.2	Perturbative approach	23
4.3	Ultrashort core-hole lifetime expansion	25

1 Introduction

In the past decade, Resonant Inelastic X-ray Scattering (RIXS) has made remarkable progress as a spectroscopic technique. This is a direct result of the availability of high-brilliance synchrotron X-ray radiation sources and of advanced photon detection instrumentation. The technique's unique capability to probe elementary excitations in complex materials by measuring their energy-, momentum-, and polarization-dependence has brought RIXS to the forefront of experimental photon science. In these lecture notes we discuss both the theoretical background of RIXS, focusing on those determining the low-energy charge, spin, orbital and lattice excitations of solids. These lecture notes are based on and to a large extent an excerpt from a recent review article [1].

Resonant Inelastic X-ray Scattering is a fast-developing experimental technique in which one scatters X-ray photons inelastically off matter. It is a *photon-in – photon-out* spectroscopy for which one can, in principle, measure the energy, momentum, and polarization change of the scattered photon. The change in energy, momentum, and polarization of the photon are transferred to intrinsic excitations of the material under study and thus RIXS provides information about those excitations. RIXS is a resonant technique in which the energy of the incident photon is chosen such that it coincides with, and hence resonates with, one of the atomic X-ray transitions of the system. The resonance can greatly enhance the inelastic scattering cross-section, sometimes by many orders of magnitude, and offers a unique way to probe charge, magnetic, and orbital degrees of freedom on selective atomic sites in a crystal. Early experimental work, and some more recent reviews include [2–9].

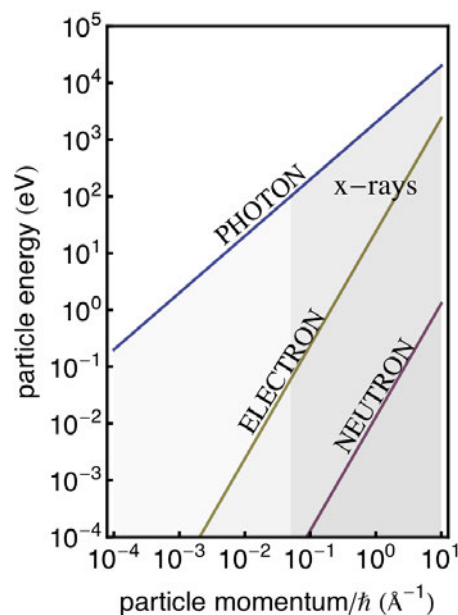


Fig. 1: (Kinetic) energy and momentum carried by the different elementary particles that are often used for inelastic scattering experiments. The scattering phase-space (the range of energies and momenta that can be transferred in a scattering event) of X-rays is indicated in blue, electrons in brown and neutrons in red.

1.1 Features of RIXS as an experimental method

Compared to other scattering techniques, RIXS has a number of unique features: it covers a huge scattering phase-space, is polarization dependent, element and orbital specific, bulk sensitive, and requires only small sample volumes. We briefly illustrate these features below and discuss them more extensively in the sections to follow.

1. RIXS exploits both the *energy and momentum* dependence of the photon scattering cross-section. Comparing the energies of a neutron, electron, and photon, each with a wavelength on the order of the relevant length scale in a solid, i.e., the interatomic lattice spacing, which is on the order of a few Angstroms, it is obvious that an X-ray photon has much more energy than an equivalent neutron or electron, see Fig. 1. The scattering phase space (the range of energies and momenta that can be transferred in a scattering event) available to X-rays is therefore correspondingly larger and is in fact without equal. For instance, unlike photon scattering experiments with visible or infrared light, RIXS can probe the full dispersion of low energy excitations in solids.
2. RIXS is *element and orbital specific*: Chemical sensitivity arises by tuning the incident photon energy to specific atomic transitions of the different types of atoms in a material. Such transitions are called absorption edges. RIXS can even differentiate between the same chemical element at sites with inequivalent chemical bondings, with different valencies or at inequivalent crystallographic positions if the absorption edges in these cases are distinguishable. In addition, the type of information that may be gleaned about the electronic excitations can be varied by tuning to different X-ray edges of the same chemical element (e.g., *K*-edge for exciting $1s$ electrons, *L*-edge for electrons in the $n = 2$ shell, or *M*-edge for $n = 3$ electrons), since the photon excites different core-electrons into different valence orbitals at each edge. The energies of these edges are shown in Fig. 2.
3. RIXS is *bulk sensitive*: the penetration depth of resonant X-ray photons is material and scattering-geometry specific, but typically it is on the order of a few μm for photons of 10 keV in the hard X-ray regime, and on the order of 0.1 μm for photons of 1 keV in the soft X-ray regime.
4. RIXS needs only *small sample volumes*: the photon-matter interaction is relatively strong, compared to, for instance, the neutron-matter interaction strength. In addition, photon sources deliver many orders of magnitude more particles per second, in a much smaller spot, than do neutron sources. These facts make RIXS possible on very small volume samples, thin films, surfaces, and nano-objects, in addition to bulk single crystal or powder samples.
5. RIXS can utilize the *polarization* of the photon: the nature of the excitations created in the material can be disentangled through polarization analysis of the incident and scattered

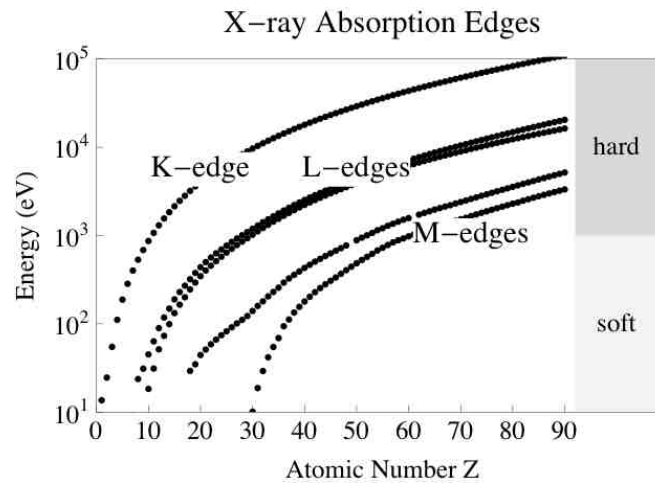


Fig. 2: Energy of the K , L_1 , L_3 , M_1 , and M_5 X-ray absorption edges as a function of atomic number Z . X-ray energies below 1 keV are referred to as soft, above as hard.

photons, which allows one, through the use of various selection rules, to characterize the symmetry and nature of the excitations. To date, very few experimental facilities allow the polarization of the scattered photon to be measured [10, 11], though the incident photon polarization is frequently varied. It is important to note that a polarization change of a photon is necessarily related to an angular momentum change. Conservation of angular momentum means that any angular momentum lost by the scattered photons has been transferred to elementary excitations in the solid.

In principle RIXS can probe a very broad class of intrinsic excitations of the system under study, as long as these excitations are overall charge-neutral. This constraint arises from the fact that in RIXS the scattered photons do not add or remove charge from the system under study. In principle then, RIXS has a finite cross-section for probing the energy, momentum and polarization dependence of, for instance, the electron-hole continuum and excitons in band metals and semiconductors, charge transfer and $d-d$ -excitations in strongly correlated materials, lattice excitations and so on. In addition magnetic excitations are also symmetry-allowed in RIXS, because the orbital angular momentum that the photons carry can in principle be transferred to the electron's spin angular momentum. This versatility of RIXS is an advantage and at the same time a complicating factor, because different types of excitations will generally be present in a single RIXS spectrum.

The generic advantages of the RIXS technique listed above perhaps raise the question as to why this spectroscopic technique is not as widely used as, say, angle-resolved photoemission (ARPES) or neutron scattering. The main limitation is that the RIXS process is photon-hungry, i.e., it requires a substantial incident photon flux to obtain enough scattered photons to collect spectra with a high enough resolution in energy and momentum in a reasonable time. With a required resolving power (defined as the incident photon energy divided by the energy resolution) of four orders of magnitude, RIXS has been a real challenge. Up until a few years ago this has limited RIXS experiments to measuring energy losses on the order of half an electron

volt or greater. Thus neutron scattering and ARPES offered a more direct examination of the low energy excitations near the Fermi level. However, recent progress in RIXS instrumentation has been dramatic and this situation is now changing. One of the purposes of these notes is to summarize this progress which is beginning to elevate RIXS into an important condensed matter physics tool for probing elementary excitations in solids.

1.2 Progress of RIXS in the last decades

As discussed above, the generic features of RIXS make it, in principle, an attractive technique to study the intrinsic momentum dependent, low-energy response of a material. However there are of course practical limitations. The most critical of these is the energy resolution, which is determined both by the availability of the instrumentation necessary to energy-resolve the photons, and by the availability of tunable photon sources of sufficient intensity.

In order to tune the incident photon energy to a particular edge, a tunable X-ray photon source is essential. This can be achieved with synchrotron radiation sources and their increase in brilliance over the past decades has been many orders of magnitudes in the 10^3 - 10^4 eV X-ray regime. The next generation photon sources include X-ray free electron lasers (FELs), which are coming on line at the time of writing. The peak brilliance of these sources is again orders of magnitude larger than that of the third generation synchrotrons and it is likely that these sources will provide further advances, particularly for time-resolved experiments.

This vast increase in photon flux has been matched by advances in the RIXS instrumentation: the monochromators, analyzers, and spectrometers. The resulting increase in resolution of RIXS experiments over time, as measured for instance at the hard X-ray Cu K - and soft X-ray Cu L_3 -edges, has greatly improved in the past decade. In concert with the great progress in the RIXS experiments, there has been a similarly rapid advance in the theoretical understanding of the scattering process and of the dynamic correlation functions that the technique probes. Taken together, the theoretical and experimental advances have driven an enormous increase in the number of RIXS-related publications.

It seems likely that this strong growth will continue. First, because of the ongoing push to better energy resolutions. Second, and perhaps more importantly, because there are a multitude of different X-ray absorption edges, in particular for the heavier elements in the periodic table, and each one of these can, in principle, be exploited for RIXS measurements. The bulk of RIXS data so far has been collected at $3d$ transition metal and oxygen edges. This is motivated by the intense scientific interest in strongly correlated transition-metal oxides such as the high- T_c cuprate superconductors and the colossal magnetoresistance manganites. This focus on transition-metal oxides is an accident of history. It has been very beneficial to the field, driving advances in instrumentation and theory at the relevant edges, but there is clearly a huge potential for growth as interest moves on to other materials and other fields.

1.3 Probing elementary excitations with RIXS

The elementary excitations of a material determine many of its important physical properties, including transport properties and its response to external perturbations. Understanding the excitation spectrum of a system is key to understanding the system.

In this respect strongly correlated electron materials, e.g. transition-metal oxides, are of special interest because the low-energy electronic properties are determined by high-energy electron-electron interactions (energies on the order of eV's). From these strong interactions and correlations a set of quantum many-body problems emerge, the understanding of which lies at the heart of present day condensed matter physics. Most often this many-body physics is captured in model Hamiltonians, the exact parameters of which must be determined experimentally. RIXS, along with other spectroscopic techniques, can play an important role there, though we note that it is a spectroscopic technique applicable to many other materials and is, of course, not limited to correlated systems.

In the following, we discuss the relevant excitation energy and momentum scale on which RIXS can probe the excitation spectrum of a solid. We then briefly introduce the kinds of elementary excitations that are accessible to RIXS.

Excitation Energy and Momentum Scale As is shown in Fig. 3, the elementary excitation spectrum in solids spans the range from plasmons and charge transfer excitations at a few eV, determining for instance optical properties, through excitons, $d-d$ excitations and magnons down to phonons at the meV scale. In principle, RIXS can measure the momentum-dependence of the excitation energy of all these modes, i.e. their dispersion, because the photon transfers momentum as well as energy to the material under study.

This is unusual if one is accustomed to optical light scattering, such as Raman scattering [12]. Photons in the visible range of the spectrum with an energy of a few eV carry negligible momentum compared to the quasi-momentum of the elementary excitations of a solid (Fig. 1). A photon of 2 eV has a momentum of roughly $\hbar q = 10^{-27}$ kg m/s, or a wavevector $q = 10^{-3} \text{ \AA}^{-1}$ whereas elementary excitations in a crystal with a lattice constant of say 3 \AA have wavevectors up to $q = 2\pi/3 \approx 2 \text{ \AA}^{-1}$. On this scale optical light scattering is in essence a zero momentum probe. To measure the dispersion of elementary excitations for momenta in a sizable portion of a typical Brillouin zone, X-rays with energy on the order of 1 keV or more are needed, corresponding to, for instance, the Cu L -edge.

Overview of elementary excitations In this paragraph we briefly discuss the different elementary excitations accessible to RIXS.

Plasmons. Collective density oscillations of an electron gas are referred to as plasmons. They can be observed by inelastic X-ray scattering (IXS) or by optical probes since they occur at finite energy for $q=0$. Plasmon-like excitations were also observed early on in RIXS [13], but their resonant enhancement with respect to IXS is weak, and little work has been done since.

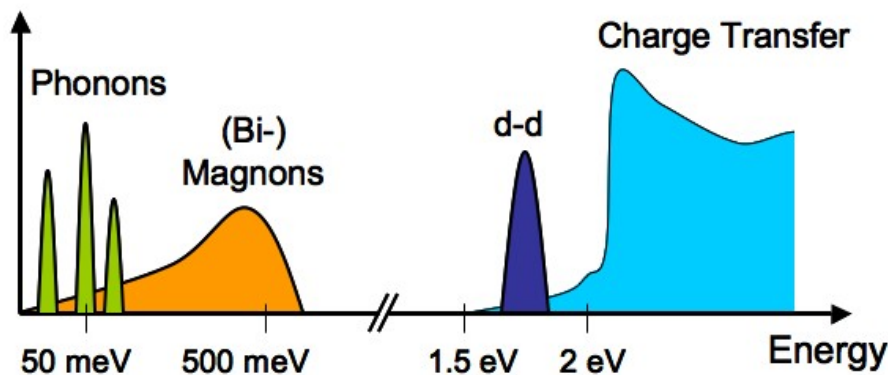


Fig. 3: Different elementary excitations in condensed matter systems and their approximate energy scales in strongly correlated electron materials such as transition-metal oxides.

Charge-transfer excitations. Charge transport in a condensed matter system is determined by the energetics of moving electrons from one site to another. In a transition-metal oxide, there are two relevant energy scales for this process. The first is the energy associated with an electron hopping from a ligand site to a metal site. This is known as the charge transfer energy, Δ , where $\Delta = E(d^{n+1}\underline{L}) - E(d^n)$, and \underline{L} represents a hole on the ligand site. The second energy scale is the energy, U , associated with moving a d -electron from one metal site to another where $U = E(d^{n+1}) + E(d^{n-1}) - 2E(d^n)$. Strongly correlated insulators may be classified by which of these two energies is the larger [14]. If $U > \Delta$, then the gap is of the charge transfer type and the system is said to be a charge-transfer insulator. Conversely, if $U < \Delta$, then the gap is controlled by the d - d Coulomb energy and the system is said to be a Mott-Hubbard insulator.

The bulk of the interesting transition metal oxide compounds, including the cuprates, nickelates and manganites are all in the charge transfer limit. This means the lowest lying excitations across the optical gap are charge transfer excitations and therefore these are of central importance in these materials. Key questions include the size of the gap (typically on the order of a few eV) and the nature of the excitations: Do they form bound exciton states? Are these localized or can they propagate through the lattice? What are their lifetimes, symmetries, and temperature dependence, etc. While some studies have been performed using other techniques, notably EELS and optical conductivity measurements, RIXS offers a powerful probe for many of these questions and has been applied extensively.

Crystal-field and orbital excitations. Many strongly correlated systems exhibit an orbital degree of freedom, that is, the valence electrons can occupy different sets of orbitals. Orbitorally active ions are also magnetic: they have a partially filled outer shell. This orbital degree of freedom determines many physical properties of the solid, both directly, and also indirectly because the orbitals couple to other degrees of freedom. For instance, the orbital's charge distribution couples to the lattice, and according to the Goodenough-Kanamori rules for superexchange the orbital order also determines the spin-spin interactions. The nature of the orbital degree of freedom, i.e., the orbital ground state and its excitations, are an important aspect of strongly correlated systems.

In many Mott insulators this orbital physics is governed by the crystal field: the levels of the orbitally active ion are split and the orbital ground state is uniquely determined by local, single-ion considerations. The orbital excitations from this ground state are transitions between the crystal field levels. Crystal field transitions between different d -orbitals are called d - d excitations. Such excitations are currently routinely seen by RIXS and are now well understood.

In other cases the crystal field does not split the levels of the outer shell very much, leaving an orbital (quasi-)degeneracy in the ground state. This local low-energy degree of freedom can couple to orbital degrees of freedom on neighboring sites by superexchange processes, and in this way collective orbital excitations can emerge. The quanta of these collective modes are called orbitons, in analogy to spin waves and magnons. Definitive proof of the existence of orbitons remains elusive. RIXS is contributing significantly to the search for orbitons.

Magnetic excitations. Magnetism and long-range magnetic ordering are arguably the best known and most studied consequences of the electron-electron interactions in solids. When usual magnetic order sets in, be it either of ferro-, ferri-, or antiferromagnetic type, the global spin rotation symmetry in the material is broken. As a result characteristic collective magnetic excitations emerge. The resulting low-energy quasiparticles, the magnons, and the interactions between them determine all low temperature magnetic properties. Magnon energies can extend up to ~ 0.3 eV (e.g. in cuprates) and their momenta up to $\sim 1 \text{ \AA}^{-1}$. Recently magnon dispersions have been measured for the first time at the Cu L -edge on thin films of La_2CuO_4 [15]. In K -edge RIXS bi-magnon excitations and their dispersions have also been observed [16].

A melting of the long-range ordering, for instance through an increase in quantum fluctuations as a result of the introduction of mobile charge carriers in a localized spin system, or by the frustration of magnetic interactions between the spins, can result in the formation of spin-liquid ground states. Spin liquids potentially have elusive properties such as high-temperature superconductivity or topological order, which one is only beginning to explore and understand. Some of the more exotic magnetic excitations that emerge from these ground states, such as spinons and triplons can also be observed by RIXS [17].

Phonons. Phonons are the quantized lattice vibration modes of a periodic solid. These are bosonic modes with energies typically below 0.1 eV, so that the detection of single phonon excitations is only just possible with present day RIXS resolution. Therefore phonon loss features were resolved for the first time with RIXS only very recently, at the Cu L - [15] and K -edge [18]. In addition anomalous features in CuB_2O_4 have been qualitatively described by extending the electron-only considerations to include the lattice degrees of freedom [19]. Theoretically, the study of phonons in RIXS promises quantitative investigations of the electron-phonon coupling [20].

2 The RIXS process

The microscopic picture of the resonant inelastic X-ray scattering process is most easily explained in terms of an example. We will choose a copper-oxide material as a typical example, but it should be stressed once more that the focus of RIXS on transition-metal oxides is

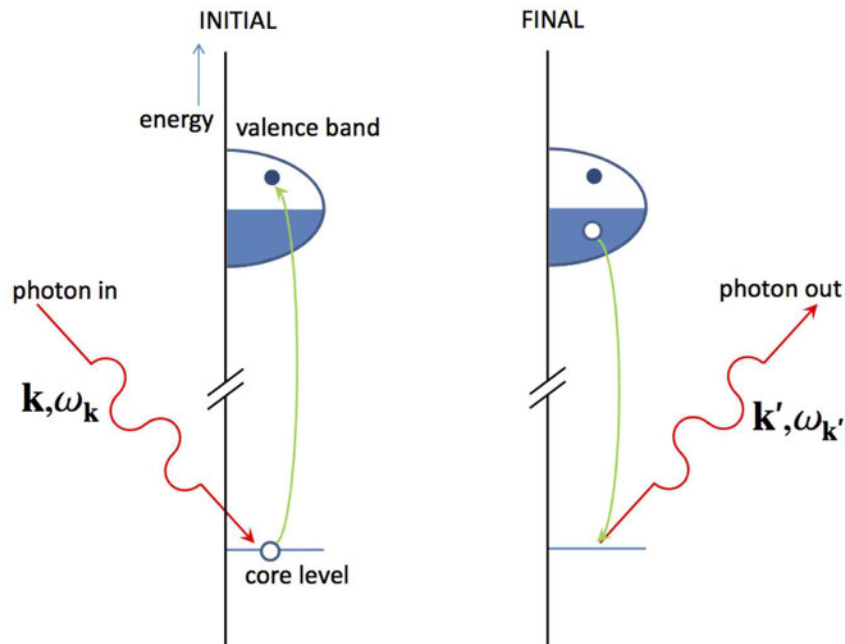


Fig. 4: In a direct RIXS process the incoming X-rays excite an electron from a deep-lying core level into the empty valence. The empty core state is then filled by an electron from the occupied states under the emission of an X-ray. This RIXS process creates a valence excitation with momentum $\hbar\mathbf{k}' - \hbar\mathbf{k}$ and energy $\hbar\omega_{\mathbf{k}'} - \hbar\omega_{\mathbf{k}}$.

something of an accident of history and is not a fundamental limitation of the technique. In a copper-oxide material, one can tune the incoming photon energy to resonate with the copper K , L , or M absorption edges, where in each case the incident photon promotes a different type of core electron into an empty valence shell, see Figs. 4 and 5. The electronic configuration of Cu^{2+} is $1s^2 2s^2 2p^6 3s^2 3p^6 3d^9$, with the partially filled $3d$ valence shell characteristic of transition metal ions. The copper K -edge transition $1s \rightarrow 4p$, is around 9000 eV and in the *hard X-ray* regime. The $L_{2,3}$ -edge $2p \rightarrow 3d$ (~ 900 eV) and $M_{2,3}$ -edge $3p \rightarrow 3d$ (~ 80 eV) are *soft X-ray* transitions. Alternatively, by tuning to the Oxygen K -edge, one can choose to promote an O $1s$ to an empty $2p$ valence state, which takes ~ 500 eV.

After absorbing a soft or hard X-ray photon, the system is in a highly energetic, unstable state: a hole deep in the electronic core is present. The system quickly decays from this intermediate state, typically within 1–2 femtoseconds. Decay is possible in a number of ways, for instance via an Auger process, where an electron fills the core hole while simultaneously emitting another electron. This non-radiative decay channel is not relevant for RIXS, which instead is governed by fluorescent decay, in which the empty core-state is filled by an electron and at the same time a photon is emitted.

There are two different scattering mechanisms by which the energy and momentum of the emitted photon can change from the incident one. These are known as *direct* and *indirect* RIXS. The distinction between these two is discussed below.

2.1 Direct and indirect RIXS

Resonant inelastic X-ray scattering processes are classified as either direct or indirect [21, 22]. This distinction is useful because the cross-sections for each are quite different. When direct scattering is allowed, it is the dominant inelastic scattering channel, with indirect processes contributing only in higher order. In contrast, for the large class of experiments for which direct scattering is forbidden, RIXS relies exclusively on indirect scattering channels.

Direct RIXS For direct RIXS, the incoming photon promotes a core-electron to an empty valence band state, see Fig. 4. Subsequently an electron from a *different* state in the valence band decays and annihilates the core hole.

The net result is a final state with an electron-hole excitation, since an electron was created in an empty valence band state and a hole in the filled valence band. The electron-hole excitation can propagate through the material, carrying momentum $\hbar\mathbf{q}$ and energy $\hbar\omega$. Momentum and energy conservation require that $\mathbf{q} = \mathbf{k}' - \mathbf{k}$ and $\omega = \omega_{\mathbf{k}'} - \omega_{\mathbf{k}}$, where $\hbar\mathbf{k}$ ($\hbar\mathbf{k}'$) and $\hbar\omega_{\mathbf{k}}$ ($\hbar\omega_{\mathbf{k}'}$) are the momentum and energy of the incoming (outgoing) photon, respectively.

For direct RIXS to occur, both photoelectric transitions, the initial one from core to valence state and succeeding one from conduction state to fill the core hole, must be allowed. These transitions can for instance be an initial dipolar transition of $1s \rightarrow 2p$ followed by the decay of another electron in the $2p$ band from $2p \rightarrow 1s$, in for example wide-band gap insulators. This happens for instance at the K -edge of oxygen, carbon, and silicon. At transition-metal L -edges, dipole transitions give rise to direct RIXS via $2p \rightarrow 3d$ absorption and subsequent $3d \rightarrow 2p$ decay. In all these cases, RIXS probes the valence and conduction states directly. Although the direct transitions into the valence shell dominate the spectral line shape, the spectral weight can be affected by interactions in the intermediate-state driven by, for example, the strong core-hole potential.

Indirect RIXS The indirect RIXS process is slightly more complicated. For pure indirect RIXS to occur, photoelectric transitions from the core-state to conduction-band states must be weak. Instead, the incoming photon promotes a core-electron into an empty state several electron volts above the Fermi level. Subsequently the electron from this same state decays to fill the core hole, see Fig. 5. The most studied example is RIXS at the transition-metal K -edges ($1s \rightarrow 4p$). Obviously, in the absence of any additional interaction, no inelastic scattering would be observed. But in the intermediate state a core hole is present, which exerts a strong potential on the $3d$ valence electrons, that therefore tend to screen the core hole. The core-hole potential scatters these valence electrons, thereby creating electron-hole excitations in the valence band. After the $4p \rightarrow 1s$ decay, the electron-hole excitations are then left behind in the system.

Indirect RIXS is thus due to shakeup excitations created by the intermediate state core hole. The fact that close to the absorption edge the $1s$ core hole and $4p$ electron bind together to form an exciton does not change this picture conceptually. In this case, one may think of the valence electrons as scattering off this exciton.

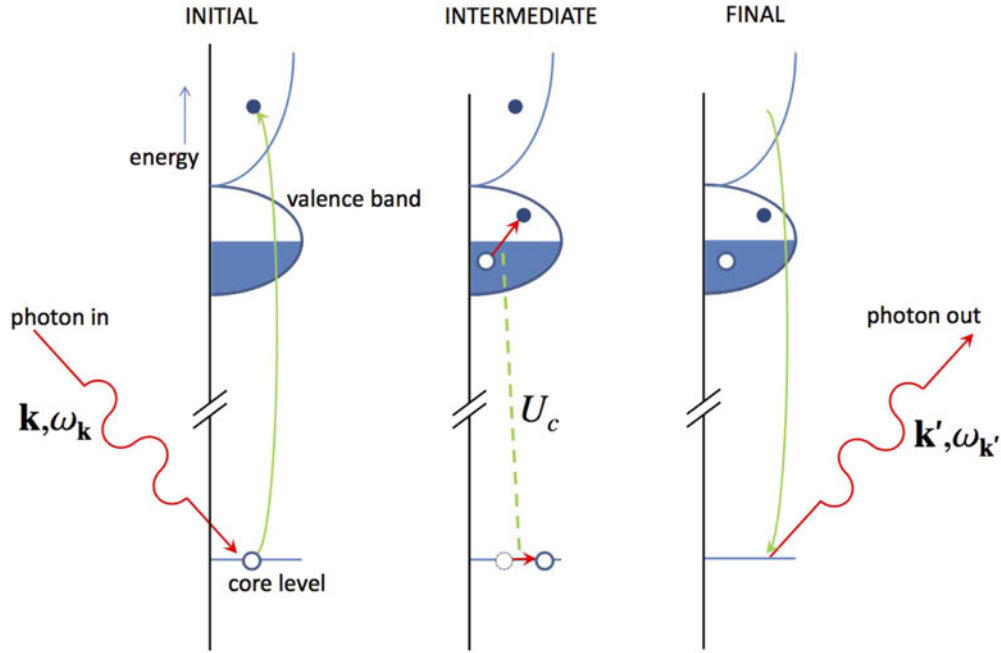


Fig. 5: In an indirect RIXS process, an electron is excited from a deep-lying core level into the valence shell. Excitations are created through the Coulomb interaction U_c between the core hole (and in some cases the excited electron) and the valence electrons.

In RIXS, the solid is taken from a ground state with energy E_g , to a final-state with excitations and an energy E_f . The energy and momentum of the excitation is determined by the difference in photon energy $\hbar\omega_k - \hbar\omega_{k'}$ and momentum $\hbar\mathbf{k}' - \hbar\mathbf{k}$, respectively. The RIXS intensity can in general be written in terms of a scattering amplitude as

$$I(\omega, \mathbf{k}, \mathbf{k}', \epsilon, \epsilon') = \sum_f |\mathcal{F}_{fg}(\mathbf{k}, \mathbf{k}', \epsilon, \epsilon', \omega_k)|^2 \delta(E_f + \hbar\omega_{k'} - E_g - \hbar\omega_k),$$

where the delta function enforces energy conservation and the amplitude $\mathcal{F}_{fg}(\mathbf{k}, \mathbf{k}', \epsilon, \epsilon', \omega_k)$ reflects which excitations are probed and how, for instance, the spectral weights of final-state excitations depend on the polarization vectors, ϵ and ϵ' of the incoming and outgoing X-rays, respectively. The following sections derive the RIXS scattering amplitude and demonstrate how it can be broken down into separate pieces.

First, we need to derive a general expression for the RIXS scattering amplitude. Section 3 looks at the interaction between photons and matter. RIXS refers to the process where the material first absorbs a photon. The system is then in a short-lived intermediate state, from which it relaxes radiatively. In an experiment, one studies the X-rays emitted in this decay process. This two-step process cannot be described simply by using Fermi's Golden Rule, but requires a higher-order treatment, known as the Kramers-Heisenberg equation [23]. Since the absorption and emission are single-photon processes, the interactions between the X-rays and the material are dominated by the terms in the cross-section proportional to $\mathbf{p} \cdot \mathbf{A}$, where \mathbf{p} is the momentum of the electrons in the material and \mathbf{A} is the vector potential of the photon. The interaction

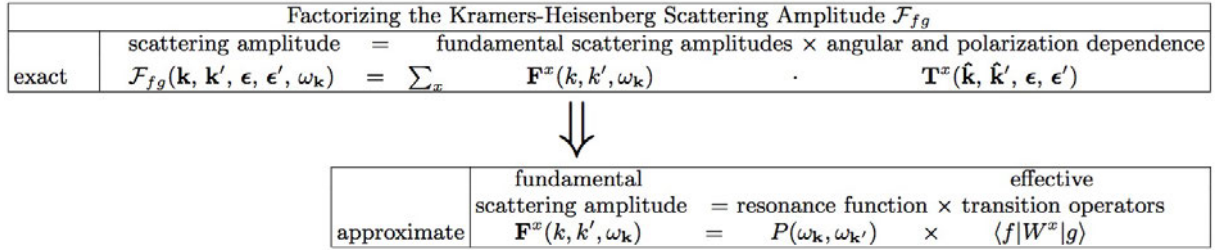


Fig. 6: In the theory of RIXS, the scattering amplitude \mathcal{F}_{fg} occurring in the Kramers-Heisenberg equation is separated into several pieces. One can split off the angular and polarization dependence \mathbf{T}^x , leaving fundamental scattering amplitudes \mathbf{F}^x . Several approximation schemes then break down these scattering amplitudes into a resonance function P and effective transition operators W^x .

between the X-rays and the material depends on external quantities, such as wavevector \mathbf{k} and polarization vectors $\boldsymbol{\epsilon}$ of the X-rays, and operators, such as \mathbf{p} and \mathbf{r} . As a result the electronic transitions are intermingled. The scattering amplitude can be split into an angular and polarization dependence $\mathbf{T}^x(\hat{\mathbf{k}}, \hat{\mathbf{k}}', \boldsymbol{\epsilon}, \boldsymbol{\epsilon}')$ related to the experimental geometry and spectral functions $\mathbf{F}^x(k, k', \omega_{\mathbf{k}})$ that measure the properties of the material, see Fig. 6. This separation can be done exactly. It is important to note that there are only a finite number of fundamental scattering amplitudes $\mathbf{F}^x(k, k', \omega_{\mathbf{k}})$ and that the RIXS scattering amplitude is a linear combination of these fundamental scattering amplitudes weighted by the angular functions $\mathbf{T}^x(\hat{\mathbf{k}}, \hat{\mathbf{k}}', \boldsymbol{\epsilon}, \boldsymbol{\epsilon}')$.

The next step is to understand the fundamental scattering amplitudes. This can be done numerically but, in addition, several authors have used approximation schemes in order to provide more insight into the scattering amplitude. Generally, the approximations involve the propagation of the system in the time between the absorption and emission processes. The schemes generally allow the separation of the fundamental scattering amplitudes into a resonance function $P(\omega_{\mathbf{k}}, \omega_{\mathbf{k}'})$ and an effective transition between ground and final states $\langle f|W^x|g \rangle$, see Fig. 6. The resonance function gives the strength of the fundamental scattering amplitude, which is a combination of radial matrix elements of the transition operators and energy denominators that describe the resonant effect as a function of $\omega_{\mathbf{k}}$. The effective transition operators create excitations in the valence shell similar to an optical excitation. In certain cases, these operators can also be related to correlation functions such as the dynamic structure factor. The approximations depend on the RIXS process. Direct RIXS is approximated by using a fast-collision approximation and indirect RIXS can be approached via perturbative methods or an ultra-short core-hole lifetime expansion, see Section 4.1.

3 Interaction of light and matter

To develop the theory of RIXS, we first need to derive the Hamiltonian that describes the interaction of the incident X-ray beam with the electrons in the sample. The interaction terms in this Hamiltonian are small, controlled by the dimensionless fine structure constant $\alpha =$

$e^2/4\pi\epsilon_0\hbar c \approx 1/137$, with $e = |e|$ the magnitude of the elementary charge and ϵ_0 the permittivity of free space. Therefore they can be treated as a perturbation to the terms in the Hamiltonian that describe the system under study. To second order in such a perturbation theory, we obtain the Kramers-Heisenberg formula, which describes RIXS very well. We need to go to second order because two interactions are needed: one to create the core hole, and one for the subsequent radiative de-excitation.

3.1 Kramers-Heisenberg cross-section

The incident X-rays are described by an electromagnetic field with vector potential $\mathbf{A}(\mathbf{r}, t)$. The coupling between such a field and electrons is given by the theory of quantum electrodynamics. It is common to start from the exactly solvable case of a single electron without potentials (\mathbf{A} and electric potential $\phi(\mathbf{r}, t)$). Then, the potentials are (perturbatively) introduced and one takes two limits. The first of these is that the electrons travel at speeds, v , small compared to the speed of light. This is a good approximation even for, e.g., copper $1s$ core electrons, where we estimate $v \sim \hbar Z/ma_0 \approx 0.21c$ with Z the atomic number for copper and a_0 the Bohr radius. At first glance, v/c might not appear small in this case, but $\gamma = 1/\sqrt{1 - v^2/c^2} \approx 1.02$ and relativistic effects are still small. The second limit is that the potentials related to both the electrons and the photons in the system are small compared to twice the mass of the electron: $e\phi/2mc^2$, $e|\mathbf{A}|/2mc \ll 1$ (m is the electron mass). Although the intrinsic potentials of materials diverge close to the nuclei, they may be treated consistently within the whole procedure for $Z \ll 137$ (see page 948 in [24]). Photon potentials at existing X-ray sources satisfy these limits. However, in the future at very strongly focussed X-ray Free Electron Lasers, the electric field of the photon is projected to exceed 10^{16} V/m, which gives $e|\mathbf{A}| \sim 2mc$ at a photon energy of ~ 8 keV so that these approximations are no longer valid. However, such effects are neglected here and the formalism is developed for non-relativistic electrons in small potentials.

In these limits, one obtains for a system with N electrons, in SI units (see pages 944–947 in [24] or pages 85–88 in [25]),

$$\begin{aligned}
 H = \sum_{i=1}^N & \left[\frac{(\mathbf{p}_i + e\mathbf{A}(\mathbf{r}_i))^2}{2m} + \frac{e\hbar}{2m} \boldsymbol{\sigma}_i \cdot \mathbf{B}(\mathbf{r}_i) \right. \\
 & \left. + \frac{e\hbar}{2(2mc)^2} \boldsymbol{\sigma}_i \cdot \left(\mathbf{E}(\mathbf{r}_i) \times (\mathbf{p}_i + e\mathbf{A}(\mathbf{r}_i)) - (\mathbf{p}_i + e\mathbf{A}(\mathbf{r}_i)) \times \mathbf{E}(\mathbf{r}_i) \right) \right] \quad (1) \\
 & + \frac{e\hbar^2 \rho(\mathbf{r}_i)}{8(mc)^2 \epsilon_0} + H_{\text{Coulomb}} + \sum_{\boldsymbol{\kappa}, \boldsymbol{\varepsilon}} \hbar \omega_{\boldsymbol{\kappa}} \left(a_{\boldsymbol{\kappa}\boldsymbol{\varepsilon}}^\dagger a_{\boldsymbol{\kappa}\boldsymbol{\varepsilon}} + \frac{1}{2} \right),
 \end{aligned}$$

where \mathbf{p}_i , \mathbf{r}_i and $\boldsymbol{\sigma}_i$ are, respectively, the momentum and position operators and the Pauli matrices acting on electron i . $\mathbf{A}(\mathbf{r})$ is the vector potential, $\mathbf{E}(\mathbf{r}) = -\nabla\phi - \partial\mathbf{A}/\partial t$, the electric field, and $\mathbf{B}(\mathbf{r}) = \nabla \times \mathbf{A}$, the magnetic field. $a_{\boldsymbol{\kappa}\boldsymbol{\varepsilon}}^{(\dagger)}$ annihilates (creates) a photon in the mode with wave vector $\boldsymbol{\kappa}$ and polarization vector $\boldsymbol{\varepsilon}$. The second term yields the Zeeman splitting, and the third includes spin-orbit coupling. The interaction of electrons with an external electric

potential and with other electrons and nuclei in the sample (including the Darwin term) are all described by H_{Coulomb} . The vector potential can be expanded in plane waves as

$$\mathbf{A}(\mathbf{r}) = \sum_{\mathbf{k}, \epsilon} \sqrt{\frac{\hbar}{2\mathcal{V}\epsilon_0\omega_{\mathbf{k}}}} \left(\epsilon a_{\mathbf{k}\epsilon} e^{i\mathbf{k}\cdot\mathbf{r}} + \epsilon^* a_{\mathbf{k}\epsilon}^\dagger e^{-i\mathbf{k}\cdot\mathbf{r}} \right), \quad (2)$$

where \mathcal{V} is the volume of the system.

In order to derive the photon scattering cross-section one splits the Hamiltonian H into an electron-photon interaction part, H' , and the remaining terms, H_0 , which describe the electron and photon dynamics in the absence of electron-photon interactions. H' is then treated as a perturbation to H_0 . To calculate the RIXS cross-section in this perturbation scheme, it is assumed that there is a single photon in the initial state with momentum $\hbar\mathbf{k}$, energy $\hbar\omega_{\mathbf{k}}$ and polarization ϵ that is scattered to $(\hbar\mathbf{k}', \hbar\omega_{\mathbf{k}'}, \epsilon')$ in the final state. Photon scattering then induces a change in the material from ground state $|g\rangle$ to final state $|f\rangle$, with energies E_g and E_f respectively. In the process, the photon loses momentum $\hbar\mathbf{q} = \hbar\mathbf{k} - \hbar\mathbf{k}'$ and energy $\hbar\omega = \hbar\omega_{\mathbf{k}} - \hbar\omega_{\mathbf{k}'}$ to the sample. Fermi's Golden Rule to second order gives the transition rate for this process :

$$w = \frac{2\pi}{\hbar} \sum_{\mathbf{f}} \left| \langle \mathbf{f} | H' | \mathbf{g} \rangle + \sum_n \frac{\langle \mathbf{f} | H' | n \rangle \langle n | H' | \mathbf{g} \rangle}{E_g - E_n} \right|^2 \delta(E_{\mathbf{f}} - E_g), \quad (3)$$

where the initial state $|\mathbf{g}\rangle = |g; \mathbf{k}\epsilon\rangle$, the intermediate state $|n\rangle$ and the final state $|\mathbf{f}\rangle = |f; \mathbf{k}'\epsilon'\rangle$ are eigenstates of H_0 with energies $E_g = E_g + \hbar\omega_{\mathbf{k}}$, E_n , and $E_{\mathbf{f}} = E_f + \hbar\omega_{\mathbf{k}'}$, respectively. The first order amplitude in general dominates the second order, but when the incoming X-rays are in resonance with a specific transition in the material ($E_g \approx E_n$), then the second order terms become large. The second order amplitude causes resonant scattering, while the first order yields non-resonant scattering.

In order to derive H' it is useful to classify the terms of Eq. (1) by powers of \mathbf{A} . Terms of H that are quadratic in \mathbf{A} are the only ones to contribute to the first order amplitude, because they contain terms proportional to $a_{\mathbf{k}'\epsilon'}^\dagger a_{\mathbf{k}\epsilon}$ and $a_{\mathbf{k}\epsilon} a_{\mathbf{k}'\epsilon'}^\dagger$. To be specific, the quadratic contribution from the first term of H gives rise to non-resonant scattering, while the third term of H yields magnetic non-resonant scattering. Although both appear in the first order scattering amplitude, they in principle also contribute to the second order, but we neglect these processes because they are of order $\alpha^{3/2}$.

The interaction terms linear in \mathbf{A} do not contribute to the first order amplitude, but do contribute to the second order. They thus give rise to resonant processes. In the following, we neglect such contributions that come from the third term of Eq. (1), because they are of second order in two separate expansions. Firstly, this term of H is of second order in the limits discussed above, and secondly, it appears in the second order of the scattering amplitude. Finally, all terms in Eq. (1) that are independent of \mathbf{A} are included in H_0 . The relevant remaining terms are

$$H' = \sum_{i=1}^N \left[\frac{e}{m} \mathbf{A}(\mathbf{r}_i) \cdot \mathbf{p}_i + \frac{e^2}{2m} \mathbf{A}^2(\mathbf{r}_i) + \frac{e\hbar}{2m} \boldsymbol{\sigma}_i \cdot \nabla \times \mathbf{A}(\mathbf{r}_i) - \frac{e^2\hbar}{(2mc)^2} \boldsymbol{\sigma}_i \cdot \frac{\partial \mathbf{A}(\mathbf{r}_i)}{\partial t} \times \mathbf{A}(\mathbf{r}_i) \right], \quad (4)$$

where the gauge was fixed by choosing $\nabla \cdot \mathbf{A}(\mathbf{r}) = 0$ so that $\mathbf{A} \cdot \mathbf{p} = \mathbf{p} \cdot \mathbf{A}$.

The two terms of H' that contribute to the first order amplitude are the one proportional to \mathbf{A}^2 and the $\boldsymbol{\sigma} \cdot (\partial \mathbf{A} / \partial t) \times \mathbf{A}$ term. The latter is smaller than the former by a factor $\hbar \omega_{\mathbf{k}(\nu)} / mc^2 \ll 1$, and is therefore neglected. The first order term in Eq. (3) then becomes

$$\frac{e^2}{2m} \langle \mathbf{f} | \sum_i \mathbf{A}^2(\mathbf{r}_i) | \mathbf{g} \rangle = \frac{\hbar e^2}{2m \mathcal{V} \epsilon_0} \frac{\boldsymbol{\epsilon}'^* \cdot \boldsymbol{\epsilon}}{\sqrt{\omega_{\mathbf{k}} \omega_{\mathbf{k}'}}} \langle \mathbf{f} | \sum_i e^{i\mathbf{q} \cdot \mathbf{r}_i} | \mathbf{g} \rangle. \quad (5)$$

When the incident energy $\hbar \omega_{\mathbf{k}}$ is much larger than any resonance of the material, the scattering amplitude is dominated by this channel, which is called Thompson scattering. In scattering from a crystal at zero energy transfer, this term contributes amongst others to the Bragg peaks. It also gives rise to non-resonant inelastic scattering. In practice, RIXS spectra show a strong resonance behavior, demonstrating that for these processes, it is the second order term that dominates the scattering. We therefore omit the \mathbf{A}^2 contribution in the following. More details on non-resonant inelastic X-ray scattering can be found in, for instance, [8, 26].

The second order amplitude in Eq. (3) becomes large when $\hbar \omega_{\mathbf{k}}$ matches a resonance energy of the system, and the incoming photon is absorbed first in the intermediate state, creating a core hole. The denominator $E_g + \hbar \omega_{\mathbf{k}} - E_n$ is then small, greatly enhancing the second order scattering amplitude. We neglect the other, off-resonant processes here, though they do give an important contribution to non-resonant scattering [6]. The resonant part of the second order amplitude is

$$\frac{e^2 \hbar}{2m^2 \mathcal{V} \epsilon_0 \sqrt{\omega_{\mathbf{k}} \omega_{\mathbf{k}'}}} \sum_n \sum_{i,j=1}^N \frac{\langle \mathbf{f} | e^{-i\mathbf{k}' \cdot \mathbf{r}_i} (\boldsymbol{\epsilon}'^* \cdot \mathbf{p}_i - \frac{i\hbar}{2} \boldsymbol{\sigma}_i \cdot \mathbf{k}' \times \boldsymbol{\epsilon}'^*) | n \rangle}{E_g + \hbar \omega_{\mathbf{k}} - E_n + i\Gamma_n} \langle n | e^{i\mathbf{k} \cdot \mathbf{r}_j} \left(\boldsymbol{\epsilon} \cdot \mathbf{p}_j + \frac{i\hbar}{2} \boldsymbol{\sigma}_j \cdot \mathbf{k} \times \boldsymbol{\epsilon} \right) | \mathbf{g} \rangle \quad (6)$$

where a lifetime broadening Γ_n is introduced for the intermediate states. This accounts for the many non-radiative interaction terms that are not included in H' (for example Auger decay), which make the intermediate states very short lived.

Resonant scattering can thus occur via a magnetic and a non-magnetic term. An estimate shows that the latter dominates. The size of localized $1s$ copper core orbitals is $a_0/Z \approx 0.018 \text{ \AA}$ so that for 10 keV photons the exponential $e^{i\mathbf{k} \cdot \mathbf{r}}$ is close to unity and can be expanded. The non-magnetic term can induce a dipole transition of order $|\mathbf{p}| \sim \hbar Z / a_0 \sim 5.9 \cdot 10^{-23} \text{ kg m/s}$, whereas the magnetic term gives a dipole transition of order $(\mathbf{k} \cdot \mathbf{r}) \hbar |\mathbf{k}| / 2 \sim 2.5 \cdot 10^{-25} \text{ kg m/s}$. We thus ignore the magnetic term here, and the relevant transition operator for the RIXS cross-section is

$$\mathcal{D} = \frac{1}{im\omega_{\mathbf{k}}} \sum_{i=1}^N e^{i\mathbf{k} \cdot \mathbf{r}_i} \boldsymbol{\epsilon} \cdot \mathbf{p}_i, \quad (7)$$

where a prefactor has been introduced for convenience in the following expressions.

The double-differential cross-section $I(\omega, \mathbf{k}, \mathbf{k}', \boldsymbol{\epsilon}, \boldsymbol{\epsilon}')$ is now obtained by multiplying by the density of photon states in the solid angle $d\Omega$ ($= \mathcal{V} k'^2 d|\mathbf{k}'| d\Omega / (2\pi)^3$) and dividing by the incident flux c/\mathcal{V} [25, 6, 8]

$$I(\omega, \mathbf{k}, \mathbf{k}', \boldsymbol{\epsilon}, \boldsymbol{\epsilon}') = r_e^2 m^2 \omega_{\mathbf{k}'}^3 \omega_{\mathbf{k}} \sum_{\mathbf{f}} |\mathcal{F}_{fg}(\mathbf{k}, \mathbf{k}', \boldsymbol{\epsilon}, \boldsymbol{\epsilon}', \omega_{\mathbf{k}}, \omega_{\mathbf{k}'})|^2 \delta(E_g - E_f + \hbar\omega), \quad (8)$$

where the classical electron radius $r_e = \frac{1}{4\pi\epsilon_0} \frac{e^2}{mc^2}$. The scattering amplitude at zero temperature is given by

$$\mathcal{F}_{fg}(\mathbf{k}, \mathbf{k}', \epsilon, \epsilon', \omega_{\mathbf{k}}, \omega_{\mathbf{k}'}) = \sum_n \frac{\langle f | \mathcal{D}'^\dagger | n \rangle \langle n | \mathcal{D} | g \rangle}{E_g + \hbar\omega_{\mathbf{k}} - E_n + i\Gamma_n}, \quad (9)$$

where the prime in \mathcal{D}' indicates it refers to transitions related to the outgoing X-rays. Eqs. (8) and (9) are referred to as the Kramers-Heisenberg equations, which are generally used to calculate the RIXS cross-section.

Alternatively, we can rewrite the denominator for the intermediate-states in terms of a Green function, which is also referred to as the intermediate-state propagator, which describes the system in the presence of a core hole:

$$G(z_{\mathbf{k}}) = \frac{1}{z_{\mathbf{k}} - H} = \sum_n \frac{|n\rangle\langle n|}{z_{\mathbf{k}} - E_n}, \quad (10)$$

where $|n\rangle$ forms a complete basis set and

$$z_{\mathbf{k}} = E_g + \hbar\omega_{\mathbf{k}} + i\Gamma, \quad (11)$$

where Γ is taken to be independent of the intermediate states. The quantity $z_{\mathbf{k}}$ is the energy of the initial state combined with the finite lifetime of the core hole. In the following we will often suppress the explicit label \mathbf{k} of $z_{\mathbf{k}}$ and denote it simply by z , with an implicit incident energy dependence. With the core-hole propagator G and transition operators \mathcal{D} in place, the RIXS scattering amplitude \mathcal{F}_{fg} finally reduces to the elegant expression

$$\mathcal{F}_{fg} = \langle f | \mathcal{D}'^\dagger G(z_{\mathbf{k}}) \mathcal{D} | g \rangle. \quad (12)$$

3.2 Scattering amplitude in dipole approximation

In the previous section, Eqs. (8) and (9) give the Kramers-Heisenberg expression for RIXS. The next step is to separate the part pertaining to the geometry of the experiment from the fundamental scattering amplitudes that relate to the physical properties of the system, see Fig. 6. In addition, better-defined transition operators will be obtained. Due to the complexity of the multipole expansion, we first give a derivation in the dipole limit allowing the reader to better follow the arguments. In the next section, we present the higher order transitions.

In the dipole limit, one assumes that $e^{i\mathbf{k}\cdot\mathbf{r}_i} \cong e^{i\mathbf{k}\cdot\mathbf{R}_i}$ where \mathbf{R}_i indicates the position of the ion to which electron i is bound. Note that \mathbf{R}_i is not an operator. This has as a result that the electronic transitions are due to the momentum operator \mathbf{p} and Eq. (7) becomes

$$\mathcal{D} = \epsilon \cdot \mathbf{D} \quad \text{with} \quad \mathbf{D} = \frac{1}{im\omega_{\mathbf{k}}} \sum_{i=1}^N e^{i\mathbf{k}\cdot\mathbf{R}_i} \mathbf{p}_i. \quad (13)$$

Generally, the matrix elements are expressed in terms of the position operator \mathbf{r} . For example, in the absorption step, one can write

$$\begin{aligned} \langle n | \mathbf{D} | g \rangle &= \sum_{i=1}^N \frac{e^{i\mathbf{k} \cdot \mathbf{R}_i}}{im\omega_{\mathbf{k}}} \langle n | \mathbf{p}_i | g \rangle = \sum_{i=1}^N \frac{e^{i\mathbf{k} \cdot \mathbf{R}_i}}{\hbar\omega_{\mathbf{k}}} \langle n | \left[\frac{\mathbf{p}_i^2}{2m}, \mathbf{r}_i \right] | g \rangle \\ &\cong \sum_{i=1}^N \frac{e^{i\mathbf{k} \cdot \mathbf{R}_i}}{\hbar\omega_{\mathbf{k}}} (E_n - E_g) \langle n | \mathbf{r}_i | g \rangle \cong \sum_{i=1}^N e^{i\mathbf{k} \cdot \mathbf{R}_i} \langle n | \mathbf{r}_i | g \rangle, \end{aligned}$$

where $\hbar\omega_{\mathbf{k}} \cong E_n - E_g$. The operator thus reduces to the dipole operator $\mathbf{D} = \sum_{i=1}^N e^{i\mathbf{k} \cdot \mathbf{R}_i} \mathbf{r}_i$ that causes electronic transitions.

The next step is to separate the part that pertains to the geometry of the experiment (the polarization vectors ϵ' and ϵ) from the physical properties of the system. Ultimately, our interest lies in the spectral functions of a material. The geometry is chosen in an optimal way to measure them. Using spherical-tensor algebra, we can rewrite the scattering amplitude, Eq. (12), remaining in the dipole limit, Eq. (13), as

$$\mathcal{F}_{fg} = \sum_{x=0}^2 [x] n_{11x}^2 \langle f | [\epsilon'^*, \epsilon]^x \cdot [\mathbf{D}^\dagger, G(z_{\mathbf{k}})\mathbf{D}]^x | g \rangle,$$

using the shorthand $[l_1 \cdots l_n] = (2l_1 + 1) \cdots (2l_n + 1)$; n_{11x} is a normalization constant, and $[\ ,]^x$ is a tensor product. Since the tensor product couples tensors of rank 1 (the polarization vectors and the position vector \mathbf{r}), the rank x of the tensor products can assume the values 0, 1, and 2. The fundamental scattering amplitudes are given by

$$\mathbf{F}^x(z_{\mathbf{k}}) = \langle f | [\mathbf{D}^\dagger, G(z_{\mathbf{k}})\mathbf{D}]^x | g \rangle. \quad (14)$$

For each value of x , there are $2x + 1$ components F_q^x with $q = -x, -x + 1, \dots, x$. Note that, whereas there is an infinite number of different scattering amplitudes, for dipole transitions, there are only nine fundamental ones ($3 \times 3 = 1 + 3 + 5 = 9$). All the other possible scattering amplitudes are combinations of these fundamental scattering amplitudes with a weighting determined by the angular dependence

$$\mathbf{T}^x(\epsilon, \epsilon') = [x] n_{11x}^2 [\epsilon'^*, \epsilon]^x, \quad (15)$$

which again has nine components $T_q^x(\epsilon, \epsilon')$. For $x = 0, 1$, the angular dependence is given by the inner product, $T_0^0(\epsilon, \epsilon') = \frac{1}{3} \epsilon'^* \cdot \epsilon$, and the outer product, $T_\alpha^1(\epsilon, \epsilon') = \frac{1}{2} (\epsilon'^* \times \epsilon)_\alpha$ of the polarization vectors, respectively. The total scattering amplitude in the dipole limit can now be written as

$$\mathcal{F}_{fg}(\epsilon, \epsilon', \omega_{\mathbf{k}}) = \sum_{x=0}^2 \mathbf{T}^x(\epsilon, \epsilon') \cdot \mathbf{F}^x(z_{\mathbf{k}}). \quad (16)$$

The spectra for different x and q are combinations of the spectra for different polarizations. Usually, the scattering amplitudes are calculated in terms of the components D_α of the dipole operator, where $\alpha = 1, 0, -1$ in spherical symmetry or $\alpha = x, y, z$ in Cartesian coordinates.

The spectra for different polarizations are then combined to form the fundamental scattering amplitudes. This can be compared with X-ray absorption. The circular dichroic spectrum (the $x = 1$ fundamental spectrum for X-ray absorption) is usually calculated by subtracting the spectra for left and right circularly polarized light ($\alpha = \pm 1$). The scattering amplitudes in terms of the components of the dipole operator are given by

$$F_{\alpha'\alpha} = \langle f | D_{\alpha'}^\dagger G(z_{\mathbf{k}}) D_\alpha | g \rangle = \sum_n \frac{\langle f | D_{\alpha'}^\dagger | n \rangle \langle n | D_\alpha | g \rangle}{\hbar\omega_{\mathbf{k}} + E_g - E_n + i\Gamma}. \quad (17)$$

Note that again there are only nine spectra and this is just a representation of the nine fundamental spectra in a different basis. The simplest scattering amplitude is the isotropic one given by $x = 0$. The tensor containing the isotropic scattering amplitudes F^0 has only one component F_0^0 ,

$$F_0^0 = F_{00} + F_{11} + F_{-1,-1} = F_{xx} + F_{yy} + F_{zz}, \quad (18)$$

which is just a sum of all the different polarization components. For the expressions in spherical symmetry, note that, since $r_{i\alpha'}^\dagger = (-1)^{\alpha'} r_{i,-\alpha'}$, there is no net transfer of angular momentum to the system for the isotropic scattering amplitude. Since the angular dependence is given by $\mathbf{T}^0 = \epsilon'^* \cdot \epsilon$, the isotropic contribution to the spectral line shape is removed in many experiments by the use of a 90° scattering condition with the incoming polarization vector in the scattering plane (π -polarized). This makes the incoming polarization vector perpendicular to both possible outgoing polarization vectors and therefore $\epsilon'^* \cdot \epsilon = 0$. In addition, this has the advantage that it strongly reduces the non-resonant \mathbf{A}^2 term from the experimental RIXS data (which has the same polarization dependence). This contributes mostly to the elastic line and is frequently the major experimental impediment to measuring low-energy excitations.

Tensors of rank $x = 1$ have three components. For example, the $q = 0$ component is given by

$$F_0^1 = F_{11} - F_{-1,-1} = F_{xy} - F_{yx}. \quad (19)$$

For resonant elastic X-ray scattering, the F_0^1 scattering amplitude is the one that gives rise to, amongst others, magnetic scattering. The angular dependence for $x = 1$, is given by an outer product $\mathbf{T}^1 = \epsilon'^* \times \epsilon$.

At this point it is useful to make a comparison with X-ray absorption (XAS) and resonant X-ray (elastic) scattering (RXS), which are determined by the scattering amplitude \mathcal{F}_{gg}

$$I_{\text{XAS}}(\epsilon, \omega_{\mathbf{k}}) = -\frac{1}{\pi} \text{Im} [\mathcal{F}_{gg}(\epsilon, \epsilon, \omega_{\mathbf{k}})] \quad (20)$$

$$I_{\text{RXS}}(\epsilon, \epsilon', \omega_{\mathbf{k}}) = |\mathcal{F}_{gg}(\epsilon, \epsilon', \omega_{\mathbf{k}})|^2, \quad (21)$$

where for X-ray absorption, there is only a polarization vector for the incident X-rays, and $\epsilon' \equiv \epsilon$. Since for XAS and RXS the “final” state is equivalent to the ground state in the scattering amplitude ($|f\rangle = |g\rangle$) an additional restriction is imposed on the scattering. In many symmetries, this means that only the $q = 0$ component contributes, reducing the scattering amplitude determining XAS and RXS to

$$\mathcal{F}_{gg}(\omega_{\mathbf{k}}) = \sum_{x=0}^2 T_0^x(\epsilon, \epsilon') F_0^x(z_{\mathbf{k}}). \quad (22)$$

This implies that of the $3 \times 3 = 9$ components in the full scattering amplitude, only 3 components, corresponding to $x = 0, 1, 2$ and $q = 0$, remain. For X-ray absorption, these correspond to the well-known isotropic, circular dichroic, and linear dichroic spectra, respectively.

3.3 Scattering amplitude for a multipole expansion

We next generalize the ideas from the previous section to include the different types of multipoles arising from the $\mathbf{p} \cdot \mathbf{A}$ interaction in Eq. (4). Since the dipolar and quadrupolar transitions in RIXS are predominantly excitations from a localized core hole into the valence states, the common approach is to expand the plane wave in the vector potential, see Eq. (2), around the site where the absorption takes place. Essentially, one is using an approximation of the type $e^{i\mathbf{k} \cdot \mathbf{r}_i} \cong 1 + i\mathbf{k} \cdot \mathbf{r}_i$ but in spherical harmonics. In the previous section, we treated the case that $e^{i\mathbf{k} \cdot \mathbf{r}_i} \cong 1$. The plane wave can be expanded in terms of spherical harmonics $Y_{lm}(\theta, \varphi)$ and spherical Bessel functions j_l [27]

$$e^{i\mathbf{k} \cdot \mathbf{r}_i} = 4\pi \sum_{l=0}^{\infty} \sum_{m=-l}^l i^l j_l(kr_i) Y_{lm}^*(\theta_{\hat{\mathbf{k}}}, \varphi_{\hat{\mathbf{k}}}) Y_{lm}(\theta_{\hat{\mathbf{r}}_i}, \varphi_{\hat{\mathbf{r}}_i}).$$

In order to arrive at the standard transition operators, it makes sense, at this point, to rewrite the above equation in terms of spherical tensors. A common set of tensors are the normalized spherical harmonics, which we write as the tensor $\hat{\mathbf{r}}^{(l)}$ with components $\hat{r}_m^{(l)} = \sqrt{4\pi/[l]} Y_{lm}(\theta_{\hat{\mathbf{r}}}, \varphi_{\hat{\mathbf{r}}})$. In addition, $\mathbf{r}^{(l)} = r^l \hat{\mathbf{r}}^{(l)}$. Note that $\mathbf{r}^{(0)} = 1$. For spherical harmonic tensors of order $l = 1$, the superscript is dropped $\mathbf{r} = \mathbf{r}^{(1)}$. This allows us to rewrite the expansion as

$$e^{i\mathbf{k} \cdot \mathbf{r}_i} = \sum_{l=0}^{\infty} [l] i^l j_l(kr) \hat{\mathbf{k}}^{(l)} \cdot \hat{\mathbf{r}}_i^{(l)}. \quad (23)$$

As in the previous section, we want to separate the momentum and polarization vectors of the X-rays (the geometry of the experiment) from the transitions in the material under consideration (the fundamental spectra). This can be done by recoupling the different tensors. Recoupling of the tensors [27–29] leads to

$$\mathcal{D} = \frac{1}{im\omega} \sum_{i=1}^N e^{i\mathbf{k} \cdot \mathbf{r}_i} \boldsymbol{\epsilon} \cdot \mathbf{p}_i = \frac{1}{im\omega} \sum_{i=1}^N \sum_{lL} \frac{[lL] i^l}{[l]!!} n_{1lL}^2 k^l [\mathbf{p}_i, \mathbf{r}_i^{(l)}]^L \cdot [\boldsymbol{\epsilon}, \hat{\mathbf{k}}^{(l)}]^L, \quad (24)$$

where the approximation $j_l(kr) \cong (kr)^l/[l]!!$ for $kr \ll 1$ has been used, with the double factorial $l!! = l(l-2) \cdots$. Note that the operators acting on the electrons, namely the momentum \mathbf{p}_i and position \mathbf{r}_i , are coupled together to form an effective operator \mathbf{D}^{lL} of rank $L = l-1, l, l+1$. The quantities related to the photons, namely, the wavevector \mathbf{k} and polarization $\boldsymbol{\epsilon}$ also form a tensor of rank L . Let us first consider the transition operators in Eq. (24) by introducing the transition operators [30]

$$\mathbf{D}^{lL} = \frac{p_{lL}(k)}{im\omega} \sum_{i=1}^N [\mathbf{p}_i, \mathbf{r}_i^{(l)}]^L, \quad (25)$$

with $p_{lL}(k) = [lL] n_{1lL}^2 k^l / [l]!! = 1, k/2, k/6$ for $lL = 01, 11, 12$, respectively. The values of l and L give rise to the usual dipolar ($lL = 01$), magnetic dipolar (11), and quadrupolar (12) transition operators. For $l = 0$, one has $\mathbf{r}_i^{(0)} = 1$ and the operator simplifies to $\mathbf{D}^{01} = \sum_i \mathbf{p}_i / im\omega$, which is equivalent to the dipole operator in Eq. (13) of the previous Section. In cartesian coordinates, the operator $[\mathbf{r}_i, \mathbf{p}_i]^1 = \mathbf{L}_i$ and $\mathbf{D}^{11} = \frac{\alpha a_0}{2} \sum_i \mathbf{L}_i$, with a_0 the Bohr radius and the angular momentum given in \hbar . The orbital moment forms, together with the Zeeman term in Eq. (1), the magnetic dipole transition. Since magnetic dipole transitions are of the order of $\alpha^2 = 1/137^2$, i.e., about five orders of magnitude, smaller than the electric dipole transitions of the same wavelength, they will be neglected in the remainder of this paper. The next operator is $\mathbf{D}^{12} = \frac{k}{6} \sum_{i=1}^N \mathbf{r}_i^{(2)}$ which is the electric quadrupole operator.

In the remainder, we limit ourselves to the electric L -pole transitions, and we can drop the $l = L - 1$ from the expressions, i.e., $\mathbf{D}^{L-1,L} \rightarrow \mathbf{D}^L$. The transition operators are then $\mathcal{D} \sim [\boldsymbol{\epsilon}, \mathbf{k}^{(L-1)}]^L \cdot \mathbf{D}^L$ with $\mathbf{D}^L = p_L(k) \sum_{i=1}^N \mathbf{r}_i^{(L)}$ with $L = 1, 2$ for dipolar and quadrupolar transitions, respectively. The relative strengths of the components of the multipole transition operators $r_M^{(L)}$ depend on the direction of polarization and wavevector through $[\boldsymbol{\epsilon}, \mathbf{k}^{(L-1)}]^L$. These reduce to $\boldsymbol{\epsilon}$ and $[\boldsymbol{\epsilon}, \mathbf{k}]^2$, for the electric dipolar and quadrupolar transitions, respectively. As discussed in the previous section, the part that depends on the geometry of the experiment and the fundamental spectra (9 and 25 for dipolar and quadrupolar transitions, respectively) that describe the physical properties of the system can be separated exactly. This can again be achieved by applying a recoupling on the scattering amplitude, which can then be rewritten as

$$F_{fg}(\mathbf{k}, \mathbf{k}', \boldsymbol{\epsilon}, \boldsymbol{\epsilon}', \omega_{\mathbf{k}}) = \sum_{x=0}^{2L} \mathbf{T}^{Lx}(\hat{\mathbf{k}}, \hat{\mathbf{k}}', \boldsymbol{\epsilon}, \boldsymbol{\epsilon}') \cdot \mathbf{F}^{Lx}(k, k', \omega_{\mathbf{k}}).$$

Neglecting interference effects between different multipoles, the scattering amplitude for a particular multipole is given by [30]

$$\mathbf{F}^{Lx}(k, k', \omega_{\mathbf{k}}) = \sum_n \frac{[\langle f | (\mathbf{D}^L)^\dagger | n \rangle, \langle n | \mathbf{D}^L | g \rangle]^x}{\hbar\omega_{\mathbf{k}} + E_g - E_n + i\Gamma},$$

which has angular dependence

$$\mathbf{T}^{Lx}(\hat{\mathbf{k}}, \hat{\mathbf{k}}', \boldsymbol{\epsilon}, \boldsymbol{\epsilon}') = [x] n_{LLx}^2 [[\boldsymbol{\epsilon}'^*, \hat{\mathbf{k}}'^{(L-1)}]^L, [\boldsymbol{\epsilon}, \hat{\mathbf{k}}^{(L-1)}]^L]^x.$$

The above equations give an exact separation of the Kramers-Heisenberg expression for RIXS into an angular dependence and a fundamental scattering amplitude, achieving the first step shown in Fig. 6.

In the previous section the Kramers-Heisenberg expression for the RIXS scattering amplitude \mathcal{F}_{fg} , Eq. (9), was derived and re-expressed as a product of a photon absorption operator \mathcal{D} , the intermediate state propagator G and a photon emission operator \mathcal{D}^\dagger , sandwiched between the RIXS final and ground state

$$\mathcal{F}_{fg} = \langle f | \mathcal{D}^\dagger G \mathcal{D} | g \rangle. \quad (26)$$

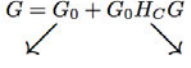
Intermediate State Propagator			
Definition	RIXS amplitude $\mathcal{F}_{fg} = \langle \mathbf{f} \mathcal{D}^\dagger G \mathcal{D} \mathbf{g} \rangle$ Intermediate State Propagator $G(z_{\mathbf{k}}) = \frac{1}{z_{\mathbf{k}} - H}$; $H = H_0 + H_C$ H_0 ground state, H_C core-hole Hamiltonian		
Exact Propagator	$G = G_0 + G_0 H_C G$ 		
	<i>Direct RIXS</i> $\mathcal{F}_{fg}^{\text{direct}} = \langle \mathbf{f} \mathcal{D}^\dagger G_0 \mathcal{D} \mathbf{g} \rangle$	<i>Indirect RIXS</i> $\mathcal{F}_{fg}^{\text{indirect}} = \langle \mathbf{f} \mathcal{D}^\dagger G_0 H_C G \mathcal{D} \mathbf{g} \rangle$	
Approximation to propagator	Fast Collision ^(a) $G(z_{\mathbf{k}}) \rightarrow 1/z_{\mathbf{k}}$	Perturbation Expansion ^(a-g) $G_0 H_C G \rightarrow G_0 H_C G_0$	Ultrashort Core-hole Life-time ^(h-j) $G_0 H_C G \rightarrow G_0 H_C G_C$
Valence excitation	caused by transition operators \mathcal{D}		caused by core-hole interaction H_C

Fig. 7: Theoretical approach to the intermediate state propagator, classifying direct and indirect RIXS processes and common approximations to the propagator: ^a [31], ^b [32], ^c [33], ^d [34], ^e [35], ^f [36], ^g [37], ^h [21], ⁱ [22], ^j [38].

The presence of the intermediate state propagator is what makes the theory of RIXS complicated – and interesting. The propagator G is defined in terms of the inverse of the total Hamiltonian H of the system, $G(z_{\mathbf{k}}) = (z_{\mathbf{k}} - H)^{-1}$, where the operator H naturally divides into the ground state Hamiltonian H_0 (governing the quantum system without a core hole) and the core-hole Hamiltonian H_C perturbing the system after photon absorption: $H = H_0 + H_C$. It should be noted that even if one commonly refers to H_C as the core-hole Hamiltonian, it also includes the interaction between the electron excited into the conduction band and the rest of the material. As core hole and excited electron together form an exciton, their separate effects on the system cannot, in principle, be disentangled.

4 Definition of direct/indirect RIXS

At this point it is useful to separate the full propagator G into the unperturbed propagator $G_0 = (z_{\mathbf{k}} - H_0)^{-1}$ and a term that contains the core-hole Hamiltonian H_C , using the identity $G = G_0 + G_0 H_C G$. This also separates the RIXS amplitude into two parts, which define *direct* and *indirect* RIXS [22]:

$$\mathcal{F}_{fg}^{\text{direct}} = \langle \mathbf{f} | \mathcal{D}^\dagger G_0 \mathcal{D} | \mathbf{g} \rangle \quad (27)$$

and

$$\mathcal{F}_{fg}^{\text{indirect}} = \langle \mathbf{f} | \mathcal{D}^\dagger G_0 H_C G \mathcal{D} | \mathbf{g} \rangle. \quad (28)$$

Note that this definition of direct/indirect RIXS, based on the Kramers-Heisenberg expression, is exact.

For the direct RIXS amplitude, the core hole does not play a role – the photon absorption and emission matrix elements determine which electronic transitions are allowed. The physical picture that arises for direct RIXS is that an incoming photon promotes a core-electron to an

empty valence state and subsequently an electron from a different state in the valence band decays, annihilating the core hole, see Fig. 4. Thus for direct RIXS to occur, both photoelectric transitions, the initial one from core to valence state and the succeeding one from valence state to fill the core hole, must be allowed. These transitions can, for example, be an initial dipolar transition of $1s \rightarrow 2p$ followed by the decay of another electron in the $2p$ band from $2p \rightarrow 1s$. This happens at the K -edge of oxygen, carbon and silicon. In addition, at transition-metal (TM) L -edges, dipole transitions causing direct RIXS are possible via $2p \rightarrow 3d$ and $3d \rightarrow 2p$ dipolar transitions. In all these cases RIXS probes the valence and conduction states directly.

For indirect RIXS, the scattering amplitude depends critically on the perturbing core-hole Hamiltonian; without it the indirect scattering amplitude vanishes. In general the scattering, $\mathcal{F}_{fg}^{\text{indirect}}$, arises from the combined influence of H_C and transition matrix elements \mathcal{D} . Most often for indirect RIXS, $\mathcal{D}/\mathcal{D}^\dagger$ create/annihilate an electron in the same state, far above the Fermi level. For instance at the TM K -edge, the $1s \leftrightarrow 4p$ process creates/annihilates an electron in $4p$ states electronvolts above the TM $3d$ valence shell. The delocalized $4p$ electron can then be approximated as being a *spectator* because (Coulomb) interactions involving the localized core hole are usually much stronger and dominate the scattering cross-section.

It should be noted that if scattering is direct, as for instance at TM L -edges, indirect processes can also contribute to the total scattering amplitude. However, as indirect scattering arises in this case as a higher order process, it is normally weaker than the leading order direct scattering amplitude. Conversely, in case of indirect RIXS, direct processes are absent by definition.

4.1 Effective theory for indirect RIXS

In the previous section, we have seen that the direct RIXS process can be written in terms of effective transition operators (see Eq. (27)) that do not involve the core-hole Hamiltonian H_C . When higher-order contributions are neglected, this approach corresponds to the fast-collision approximation, or the lowest order in the ultrashort core-hole lifetime (UCL) expansion, see Sec. 4.3. Indirect RIXS is different, as these lowest order terms do not contribute to its RIXS cross-section and the scattering process critically depends on the higher-order terms. For example, K -edge RIXS is dominated by excitations into the transition-metal $4p$ states. Since the $4p$ states are usually almost completely empty, the effective operators for direct RIXS only contribute to the elastic line, where the effective transition operator creates an electron in the valence shell in the excitation step and annihilates it again in the emission process.

Experimentally, however, RIXS is observed at the K -edge. Particularly prominent are the charge-transfer type excitations. Also the excitation of d - d transitions and magnons have been observed. The general consensus is that these excitations are created through the interaction between the valence shell and the $1s$ - $4p$ excitation created in the absorption process. Most work has focused on the interaction with the potential of the $1s$ core hole, which is known to be of the order of 6–8 eV. This potential can be written as

$$H_C = \sum_{\mathbf{k}\mathbf{k}'\mathbf{q}\mu\sigma\sigma'} U_{1s,3d} d_{\mathbf{k}+\mathbf{q},\mu\sigma}^\dagger s_{\mathbf{k}'-\mathbf{q},\sigma'}^\dagger s_{\mathbf{k}'\sigma'} s_{\mathbf{k}\mu\sigma} , \quad (29)$$

where μ sums over the different orbitals. The potential can in principle contain exchange terms, but these are negligible at the K -edge. The transient presence of this potential in the intermediate state leads to strong screening dynamics in the valence shell giving rise to the final-state excitations. This Section discusses some of the methods used to describe the excitations created by interactions in the intermediate state.

4.1.1 Momentum dependence for indirect RIXS

Recognizing that for indirect RIXS the core hole dominates the scattering process has an important consequence for the momentum dependence. In the hard X-ray regime photons have a momentum \mathbf{q} that can span several Brillouin zones because it is larger than the reciprocal lattice vectors \mathbf{G} . The photon momentum reduced to the first Brillouin zone is, by definition, $\boldsymbol{\kappa} = \mathbf{q} - n\mathbf{G}$. The translational invariance and localized nature of the core potential in Eq. (29) imply that the momentum dependence of RIXS is determined by the *reduced* momentum $\boldsymbol{\kappa}$. It will only weakly depend on $n\mathbf{G}$ as in reality a finite, but small, length-scale is associated with the core potential. RIXS spectra will therefore appear practically identical in different Brillouin zones. This is confirmed experimentally by [39]. The weak variations found in [40], are attributed by the authors to polarization effects.

This is remarkable because in IXS the *total* momentum \mathbf{q} determines the scattering amplitude. The reason for this is that in IXS \mathbf{q} enters directly into the transition matrix elements, which in RIXS are dominated by dipolar transitions for which $e^{i\mathbf{q}\cdot\mathbf{r}} \cong 1$ and that are therefore independent of \mathbf{q} . In the following, we will see how in certain limits the indirect RIXS amplitude can be related to the dynamic electronic structure factor $S_{\mathbf{k}}(\omega)$, which is directly measured by IXS. The important difference is thus that IXS measures $S_{\mathbf{q}}(\omega)$ and RIXS is, in these cases, related to $S_{\boldsymbol{\kappa}}(\omega)$.

4.2 Perturbative approach

The most straight-forward approach to include effects of the interaction H_C between the core hole and the valence shell is the use of perturbation theory. This amounts to replacing G by G_0 in Eq. (28) [32, 34, 33, 36, 35, 41], so that

$$\mathcal{F}_{fg}^{\text{indirect}} = \langle f | \mathcal{D}^\dagger G_0 H_C G_0 \mathcal{D} | g \rangle, \quad (30)$$

which is also referred to as the Born approximation and shown in terms of a Feynman diagram expansion in Fig. 8. For dipolar $1s \rightarrow 4p$ transitions at the K -edge, we have $\mathcal{D} = \sqrt{3} P_{1s,4p}^1 \sum_{\boldsymbol{\kappa} \mathbf{k} \alpha} \varepsilon_\alpha p_{\boldsymbol{\kappa}+\mathbf{k},\alpha\sigma}^\dagger s_{\boldsymbol{\kappa}\alpha\sigma}$ with $\alpha = x, y, z$, and $P_{1s,4p}^1$ the reduced matrix element containing the integral over the radial parts of the wavefunction.

In indirect RIXS, one considers the case where the $1s$ - $4p$ exciton created in the absorption step is annihilated in the emission process. Since there is a momentum transfer \mathbf{q} from the photons to the system, this implies that the momentum of the $1s$ - $4p$ exciton must have changed in the intermediate state. This can only be a result of interactions of the $1s$ - $4p$ exciton with the valence

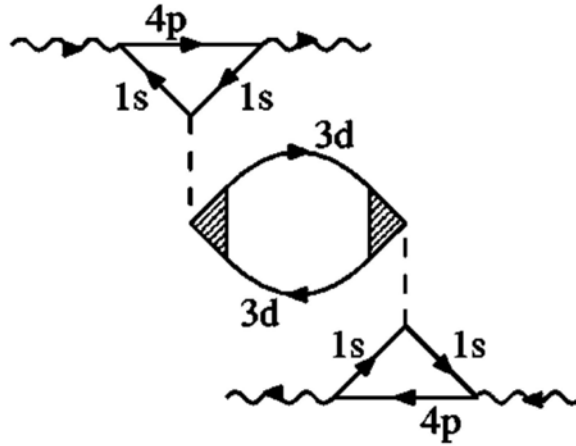


Fig. 8: Feynman diagram for the transition probability in an indirect RIXS process in the Born approximation. Green functions for Cu 1s, 4p, and 3d electrons correspond to the solid lines labeled 1s, 4p, and 3d, respectively. The wavy and broken lines represent the photon propagator and core hole potential $U_{1s,3d}$, respectively. The shaded triangle is the effective scattering vertex of the renormalized interaction between the valence electrons in the 3d-shell [36].

shell. If the dominant interaction is the Coulomb interaction of the core hole with the valence shell, then the isotropic scattering amplitude can be rewritten as [33, 8]

$$\mathcal{F}_{fg}^{\text{indirect}}(\mathbf{q}, \omega) = P(\omega_{\mathbf{k}}, \omega_{\mathbf{k}'}) T(\epsilon, \epsilon') \langle f | \rho_{\mathbf{q}} | g \rangle. \quad (31)$$

Note that all the operators involving the 1s and 4p states have been removed from the expression. The density operator is

$$\rho_{\mathbf{q}} = \sum_{\mathbf{k}\sigma} d_{\mathbf{k}+\mathbf{q},\sigma}^{\dagger} d_{\mathbf{k}\sigma}. \quad (32)$$

The resonance behavior is determined by the resonant function

$$P(\omega_{\mathbf{k}}, \omega_{\mathbf{k}'}) = 3(P_{1s,4p}^1)^2 \frac{U_{1s,3d}}{(z_{\mathbf{k}} - \hbar\omega)z_{\mathbf{k}}}, \quad (33)$$

using the fact that $\hbar\omega = \hbar\omega_{\mathbf{k}} - \hbar\omega_{\mathbf{k}'} = E_f$. The resonant function is more complex than for direct RIXS reflecting the fact that this is a higher-order excitation. The polarization dependence requires some careful consideration. In the situation where the 4p electron is a spectator an electron is excited into the 4p band with momentum \mathbf{k} and band index n and subsequently removed from the same state

$$T(\epsilon, \epsilon') = \frac{1}{N} \sum_{\mathbf{k}\alpha\alpha'} \epsilon'_{\alpha'}^* \epsilon_{\alpha} \langle 0 | p_{\mathbf{k}\alpha'} | E_{\mathbf{k}n}^{4p} \rangle \langle E_{\mathbf{k}n}^{4p} | p_{\mathbf{k}\alpha}^{\dagger} | 0 \rangle, \quad (34)$$

with $\alpha = x, y, z$. In the atomic limit, this expression reduces to $\epsilon'^* \cdot \epsilon$, since the orbital of the 4p electron is unchanged in the intermediate state. In the absence of band effects, a change in the polarization therefore implies that the angular momentum of the valence electrons has changed. However, the 4p states form wide bands that are mixtures of the different 4p orbitals, and these

local-symmetry arguments only apply at the Γ -point. Therefore, the use of a scattering condition where the incoming polarization vector is perpendicular to the outgoing polarization vectors does not necessarily imply that a symmetry change has to occur for the valence electrons. The essential physics of the material is contained in the fundamental scattering amplitude

$$F_{fg}(\mathbf{q}) = \langle f | \rho_{\mathbf{q}} | g \rangle. \quad (35)$$

This quantity is directly related to the dynamic structure factor, through

$$S_{\mathbf{q}}(\omega) = \sum_f |F_{fg}|^2 \delta(E_f - \hbar\omega) = -\frac{1}{\pi} \text{Im} \langle g | \rho_{-\mathbf{q}} \frac{1}{\hbar\omega - H + i0^+} \rho_{\mathbf{q}} | g \rangle, \quad (36)$$

which corresponds to the bubble in the Feynman diagram in Fig. 8. It should be noted that RIXS measures a projected $S_{\mathbf{q}}(\omega)$, meaning that $\rho_{\mathbf{q}}$ contains only $d_{\mathbf{k}+\mathbf{q},\sigma}^\dagger d_{\mathbf{k}\sigma}$ terms. This is a direct result of the fact that the core-hole Coulomb interaction does not scatter between different orbitals. This is different from IXS, where in principle the photon can induce a direct transition from the d states to the ligands. This does not imply that RIXS does not create charge-transfer excitations, since the charge-transfer states also have d character. In [42] multiple scattering corrections to the Born approximation are also considered on the basis of a Keldysh Green function formalism. It was found that multiple scattering effects lead to small modifications in the shape of the RIXS spectrum, which partly justifies the Born approximation for wide gap insulators such as La_2CuO_4 and NiO [43].

For direct RIXS, the detailed dependence on the polarization is given in the fundamental scattering amplitude $F_{fg,q}^x$. When including the polarization dependence for indirect RIXS, one obtains a similar fundamental scattering amplitude. The quantity F_{fg} in Eq. (35) then reduces to $F_{fg,0}^0$ and corresponds to the isotropic term. In the absence of interactions causing a transfer of angular momentum between the $4p$ and the valence shell, the indirect RIXS amplitude is simply proportional to $\rho_{\mathbf{q}}$. In terms of tensors, $\rho_{\mathbf{q}} = w_0^{dd0}(\mathbf{q})$.

A significant difference between the two processes is that when direct excitations are made into the valence shell (e.g. $2p/3p \rightarrow 3d$), the effect of the operator $w_0^{dd0} = n_h$ is relatively small, since the excited electron screens the $2p/3p$ core-hole potential very well. The isotropic contribution then mainly contributes to the elastic line. For indirect RIXS, the excited delocalized $4p$ electron does not screen the $1s$ core-hole potential very well. This produces appreciable screening dynamics of the valence electrons in the intermediate state. This is the reason why the $\rho_{\mathbf{q}}$ response generates significant inelastic scattering intensity for indirect RIXS.

4.3 Ultrashort core-hole lifetime expansion

The potential that the core hole exerts on the valence electrons is strong, the attraction $U_{1s,3d}$ between a $1s$ core hole and $3d$ electron is typically $\sim 6-8$ eV, which is of the same order as the $d-d$ Coulomb interaction $U_{3d,3d}$ that appears in Hubbard-like models. Treating such a strong interaction as a weak perturbation renders a perturbation expansion uncontrolled. To deal with the strong core-hole interaction, the Ultrashort Core-hole Lifetime (UCL) expansion

was developed in [21, 22, 38], which treats the core-hole potential as the dominating energy scale.

The UCL relies on three observations. First for most RIXS intermediate states, the core hole lifetime broadening is quite large: typically Γ is of the order of 1 eV. This yields a time scale $\tau = 1/2\Gamma = 4$ fs. Only during this ultrashort time is the system perturbed by the core hole. Many elementary excitations have an intrinsic time scale that is much larger than 4 fs. *This intrinsic timescale is the fundamental oscillation period, related to the inverse frequency ω of an excitation with energy $\hbar\omega$.* For example, phonons have a typical energy scale of up to 100 meV, and magnons of up to 250 meV, thus corresponding to timescales almost an order of magnitude larger than the core hole lifetime. Even low energy electronic valence band excitations can be within this range.

The resulting physical picture of a RIXS process involving low-energy excitations is therefore that the dynamics in the intermediate state are limited because of this lack of time, provided that the excitation time scale is not decreased significantly by the core hole. The second observation is that the core-hole potential can, to good approximation, be treated as a local potential, i.e., its dominating effect is to perturb electrons on the same atom on which the core hole resides. Finally, the core hole is considered to be immobile, which is a reliable assumption for the deep core-states such as Cu $1s$.

The calculation of the indirect RIXS amplitude within the UCL expansion by [21, 22, 38] is based on a series expansion of the Kramers-Heisenberg equation, (Eq. 9). But a Green function approach is equally viable, which then starts by inserting in Eq. (28) the identity $G = G_C + G_C H_0 G$

$$\mathcal{F}_{\mathbf{f}\mathbf{g}}^{\text{indirect}} = \langle \mathbf{f} | \mathcal{D}^\dagger G_0 H_C G_C (1 + H_0 G) \mathcal{D} | \mathbf{g} \rangle, \quad (37)$$

where the Green functions, $G_0 = (z_{\mathbf{k}} - H_0)^{-1}$, $G_C = (z_{\mathbf{k}} - H_C)^{-1}$, $G = (z_{\mathbf{k}} - H)^{-1}$, correspond to the Hamiltonian of the unperturbed system H_0 , the valence-electron core-hole interaction H_C , and the total Hamiltonian $H = H_0 + H_C$. The UCL is best illustrated by considering the core-hole Hamiltonian $H_C = U_C \sum_i \rho_i^s \rho_i^d$, where $U_C = U_{1s,3d}$ and ρ_i^s (ρ_i^d) are the density operators counting the number of $1s$ core holes ($3d$ electrons) at site i . The simplest system one can consider is one in which the $3d$ states are only occupied by either 0 or by 1 electron, for instance due to strong correlation effects in the $3d$ shell. As there is only one localized core hole present in the intermediate state, H_C then has the interesting property $H_C^l = U_C^{l-1} H_C$ for any integer $l > 0$ [21, 22], which implies that H_C is either 0 or U_C . This directly implies the relation $H_C G_C = H_C (z_{\mathbf{k}} - U_C)^{-1}$. One now obtains for the indirect RIXS amplitude

$$\mathcal{F}_{\mathbf{f}\mathbf{g}}^{\text{indirect}} = \langle \mathbf{f} | \mathcal{D}^\dagger G_0 \frac{H_C}{z_{\mathbf{k}} - U_C} (1 + H_0 G) \mathcal{D} | \mathbf{g} \rangle. \quad (38)$$

Note that this expression is exact, but of course specific for the present form of the core-hole potential; generalized forms are given in [21,22,38], which include the spin and possible orbital degrees of freedom of the $3d$ electrons.

In the leading order of the UCL expansion one retains in Eq. (38) the first order term in H_C so that

$$\mathcal{F}_{\mathbf{f}\mathbf{g}}^{\text{indirect}} = \frac{\langle \mathbf{f} | \mathcal{D}^\dagger H_C \mathcal{D} | \mathbf{g} \rangle}{(z_{\mathbf{k}} - \omega)(z_{\mathbf{k}} - U_C)} = P(\omega_{\mathbf{k}}, \omega_{\mathbf{k}'}) \langle \mathbf{f} | \rho_{\mathbf{q}}^d | \mathbf{g} \rangle, \quad (39)$$

where the resonance function

$$P(\omega_{\mathbf{k}}, \omega_{\mathbf{k}'}) = (P_{1s,4p}^1)^2 U_C ((z_{\mathbf{k}} - \omega)(z_{\mathbf{k}} - U_C))^{-1} \quad (40)$$

is introduced, and $P_{1s,4p}^1$ is the $1s \rightarrow 4p$ dipole transition amplitude. The generic shape of the resonance function depends on the form of the core-hole potential. It is remarkable that the RIXS amplitude found in leading order of the strong coupling UCL is directly related to the dynamic structure factor $S_{\mathbf{q}}(\omega)$ of Eq. (36), which is a situation very similar to the weak coupling perturbative approach, see Eq. (35). In fact for $U_C \rightarrow 0$ the strong coupling UCL resonance function reduces to the perturbative one. This result has important implications for the interpretation of RIXS spectra since this approach then suggests that with proper handling of the prefactor, RIXS can be considered as a weak probe that measures $S_{\mathbf{q}}(\omega)$.

The sub-leading contributions to the indirect UCL scattering amplitude of Eq. (38) are of the type $H_C H_0 H_C$. Such terms *a priori* cannot be reduced to a response of $\rho_{\mathbf{q}}$ because H_0 and H_C do not commute. Physically this term corresponds to an electron (or hole) hopping onto the core-hole site in the intermediate state. Denoting the hopping amplitude as t , these contributions to the scattering amplitude are down by a factor $t/(z_{\mathbf{k}} - U_C)$ with respect to the leading term. When tuning off-resonance, corrections to the UCL expansion thus become progressively smaller. On resonance these terms constitute contributions to the RIXS intensity of the order of $(t/\Gamma)^2$, which are thus governed by U_C and the inverse core-hole lifetime Γ . Corrections to the UCL are thus smaller for shorter-lived core holes. In cuprates, for instance the effective $3d$ valence bandwidth $t \approx 0.4$ eV and such corrections are expected to be moderate. For a specific system, the commutation relation for H_0 and H_C is known, and such a higher order term can be calculated explicitly and again be cast in the form of a product of a resonance function and a generalized charge response function.

The observation that within the UCL the RIXS cross-section can be factored into a resonant prefactor and the dynamic structure factor, $S_{\mathbf{q}}(\omega)$ was tested experimentally [44]. There an empirical comparison of Cu K -edge indirect RIXS spectra was reported, taken at the Brillouin-zone center, with optical dielectric loss functions measured in a number of copper oxides: Bi_2CuO_4 , CuGeO_3 , $\text{Sr}_2\text{Cu}_3\text{O}_4\text{Cl}_2$, La_2CuO_4 , and $\text{Sr}_2\text{CuO}_2\text{Cl}_2$. Analyzing both incident and scattered-photon resonances [44] extracted an incident-energy-independent response function. The overall spectral features of the indirect resonant inelastic X-ray scattering response function were found to be in a reasonable agreement with the optical dielectric loss function over a wide energy range. In the case of Bi_2CuO_4 and CuGeO_3 [44] observed that the incident-energy-independent response function, $S_{\mathbf{q}=0}(\omega)$, matches very well with the dielectric loss function, $-\text{Im}(1/\epsilon(\omega))$ measured with spectroscopic ellipsometry, suggesting that the local core-hole approximation treatment of the UCL works well in these more localized electron systems. Corner-sharing two-

dimensional copper oxides exhibit more complex excitation features than those observed in the dielectric loss functions, likely related to non-local core-hole screening effects.

The UCL expansion describes the RIXS cross-section in the limits of small and large core-hole potential. In the intermediate region, one has to resort to numerical calculations [45]. In the dynamic structure factor, excitations are created via $\rho_{\mathbf{q}}$, implying that electrons and holes are excited in an equivalent fashion. When dynamical effects are strong in the intermediate state, this can change and an asymmetry in the excitation of electron and holes can occur [45]. Since the screening electron is strongly bound to the core hole in the intermediate state, it is more likely to be scattered to higher lying states. The hole excitations on the other hand can delocalize and have a tendency to be closer to the Fermi level.

Besides charge excitations also magnetic and orbital excitations were studied with the UCL. Theoretically the two-magnon response of antiferromagnetic La_2CuO_4 was calculated within the UCL [46, 47], agreeing nicely with experiment [16]. Collective orbital excitations were investigated theoretically for LaMnO_3 [48] and for YTiO_3 [49] and compared to experiments on titanates [50].

Acknowledgments

These lecture notes are based on the review article [1], written by Luuk Ament, Michel van Veenendaal, Thomas P. Devereaux, John P. Hill, and the present lecturer. A far more complete review of the recent theoretical and in particular the experimental advances in RIXS can be found there. An excellent book that includes the theory of RIXS has been published very recently [9]. The lecturer acknowledges support from the Deutsche Forschungsgemeinschaft via SFB 1143.

References

- [1] L.J.P. Ament, M. van Veenendaal, T.P. Devereaux, J.P. Hill, and J. van den Brink, *Rev. Mod. Phys.* **83**, 705 (2011)
- [2] C.J. Sparks, *Phys. Rev. Lett.* **33**, 262 (1974)
- [3] Y.B. Bannett and I. Freund, *Phys. Rev. Lett.* **34**, 372 (1975)
- [4] P. Eisenberger, P.M. Platzman, and H. Winick, *Phys. Rev. Lett.* **36**, 623 (1976)
- [5] P. Eisenberger, P.M. Platzman, and H. Winick, *Phys. Rev. B* **13**, 2377 (1976)
- [6] M. Blume, *J. Appl. Phys.* **57**, 3615 (1985)
- [7] A. Kotani and S. Shin, *Rev. Mod. Phys.* **73**, 203 (2001)
- [8] W. Schülke: *Electron Dynamics by Inelastic X-Ray Scattering* (Oxford University Press, 2007)
- [9] M. van Veenendaal: *Theory of Inelastic Scattering and Absorption of X-rays* (Cambridge University Press, 2015)
- [10] L. Braicovich, A. Tagliaferri, E. Annese, G. Ghiringhelli, C. Dallera, F. Fracassi, A. Palenzona, and N.B. Brookes, *Phys. Rev. B* **75**, 073104 (2007)
- [11] K. Ishii, S. Ishihara, Y. Murakami, K. Ikeuchi, K. Kuzushita, T. Inami, K. Ohwada, M. Yoshida, I. Jarrige, N. Tatami, S. Niioka, D. Bizen, Y. Ando, J. Mizuki, S. Maekawa, and Y. Endoh, *Phys. Rev. B* **83**, 241101 (2011)
- [12] T.P. Devereaux and R. Hackl, *Rev. Mod. Phys.* **79**, 175 (2007)
- [13] E.D. Isaacs, P.M. Platzman, P. Metcalf, and J.M. Honig, *Phys. Rev. Lett.* **76**, 4211 (1996)
- [14] J. Zaanen, G.A. Sawatzky, and J.W. Allen, *Phys. Rev. Lett.* **55**, 418 (1985)
- [15] L. Braicovich, J. van den Brink, V. Bisogni, M. Moretti Sala, L.J.P. Ament, N.B. Brookes, G.M. De Luca, M. Salluzzo, T. Schmitt, V.N. Strocov, and G. Ghiringhelli, *Phys. Rev. Lett.* **104**, 077002 (2010)
- [16] J.P. Hill, G. Blumberg, Y.-J. Kim, D.S. Ellis, S. Wakimoto, R.J. Birgeneau, S. Komiya, Y. Ando, B. Liang, R.L. Greene, D. Casa, and T. Gog, *Phys. Rev. Lett.* **100**, 097001 (2008)
- [17] J. Schlappa, T. Schmitt, F. Vernay, V.N. Strocov, V. Ilakovac, B. Thielemann, H.M. Rønnow, S. Vanishri, A. Piazzalunga, X. Wang, L. Braicovich, G. Ghiringhelli, C. Marin, J. Mesot, B. Delley, and L. Patthey, *Phys. Rev. Lett.* **103**, 047401 (2009)

- [18] H. Yavaş, M. van Veenendaal, J. van den Brink, L.J.P. Ament, A. Alatas, B.M. Leu, M.-O. Apostu, N. Wizen, G. Behr, W. Sturhahn, H. Sinn, and E.E. Alp, *J. Phys.: Condens. Matter* **22**, 485601 (2010)
- [19] J.N. Hancock, G. Chabot-Couture, and M. Greven, *New J. Phys.* **12**, 033001 (2010)
- [20] L.J.P. Ament, M. van Veenendaal, and J. van den Brink, *Europhys. Lett.* **95**, 27008 (2011)
- [21] J. Van den Brink and M. van Veenendaal, *J. Phys. Chem. Solids* **66**, 2145 (2005)
- [22] J. Van den Brink and M. van Veenendaal, *Europhys. Lett.* **73**, 121 (2006)
- [23] H.A. Kramers and W. Heisenberg, *Z. Phys.* **48**, 15 (1925)
- [24] A. Messiah: *Quantum Mechanics, Vol. 2*
(North Holland Publishing Company, Amsterdam, 1962)
- [25] J.J. Sakurai: *Advanced Quantum Mechanics* (Addison-Wesley, 1967)
- [26] J.-P. Rueff and A. Shukla, *Rev. Mod. Phys.* **82**, 847 (2010)
- [27] D.A. Varshalovich, A.N. Moskalev, and V.K. Khersonskii:
Quantum Theory of Angular Momentum (World Scientific, 1988)
- [28] D.M. Brink and G.R. Satchler: *Angular Momentum*
(Oxford University Press, 1962)
- [29] A.P. Yutsis, I.B. Levinson, and V.V. Vanagas: *Quantum Theory of Angular Momentum*
(World Scientific, 1988)
- [30] M. Van Veenendaal and R. Benoist, *Phys. Rev. B* **58**, 3741 (1998)
- [31] J. Luo, G.T. Trammell, and J.P. Hannon, *Phys. Rev. Lett.* **71**, 287 (1993)
- [32] P.M. Platzman and E.D. Isaacs, *Phys. Rev. B* **57**, 11107 (1998)
- [33] G. Döring, C. Sternemann, A. Kaprolat, A. Mattila, K. Hämäläinen, and W. Schülke, *Phys. Rev. B* **70**, 085115 (2004)
- [34] P. Abbamonte, C.A. Burns, E.D. Isaacs, P.M. Platzman, L.L. Miller, S.W. Cheong, and M.V. Klein, *Phys. Rev. Lett.* **83**, 860 (1999)
- [35] T. Nomura and J.-I. Igarashi, *J. Phys. Soc. Jpn.* **73**, 1677 (2004)
- [36] T. Nomura and J.-I. Igarashi, *Phys. Rev. B* **71**, 035110 (2005)
- [37] R.S. Markiewicz and A. Bansil, *Phys. Rev. Lett.* **96**, 107005 (2006)

- [38] L.J.P. Ament, F. Forte, and J. van den Brink, *Phys. Rev. B* **75**, 115118 (2007)
- [39] Y.-J. Kim, J.P. Hill, S. Wakimoto, R.J. Birgeneau, F.C. Chou, N. Motoyama, K.M. Kojima, S. Uchida, D. Casa, and T. Gog, *Phys. Rev. B* **76**, 155116 (2007)
- [40] G. Chabot-Couture, J.N. Hancock, P.K. Mang, D.M. Casa, T. Gog, and M. Greven, *Phys. Rev. B* **82**, 035113 (2010)
- [41] T. Semba, M. Takahashi, and J.-I. Igarashi, *Phys. Rev. B* **78**, 155111 (2008)
- [42] J.-I. Igarashi, T. Nomura, and M. Takahashi, *Phys. Rev. B* **74**, 245122 (2006)
- [43] M. Takahashi, J.-I. Igarashi, and T. Nomura, *Phys. Rev. B* **75**, 235113 (2007)
- [44] J. Kim, D.S. Ellis, H. Zhang, Y.-J. Kim, J.P. Hill, F.C. Chou, T. Gog, and D. Casa, *Phys. Rev. B* **79**, 094525 (2009)
- [45] K.H. Ahn, A.J. Fedro, and M. van Veenendaal, *Phys. Rev. B* **79**, 045103 (2009)
- [46] J. Van den Brink, *Europhys. Lett.* **80**, 47003 (2007)
- [47] F. Forte, L.J.P. Ament, and J. van den Brink, *Phys. Rev. B* **77**, 134428 (2008)
- [48] F. Forte, L.J.P. Ament, and J. van den Brink, *Phys. Rev. Lett.* **101**, 106406 (2008)
- [49] L.J.P. Ament and G. Khaliullin, *Phys. Rev. B* **81**, 125118 (2010)
- [50] C. Ulrich, L.J.P. Ament, G. Ghiringhelli, L. Braicovich, M. Moretti Sala, N. Pezzotta, T. Schmitt, G. Khaliullin, J. van den Brink, H. Roth, T. Lorenz, and B. Keimer, *Phys. Rev. Lett.* **103**, 107205 (2009)

